coatings

MDPI

Article

Effect of Voltage Pulse Width and Synchronized Substrate Bias in High-Power Impulse Magnetron Sputtering of Zirconium Films

Chin-Chiuan Kuo [1,*], Chun-Hui Lin [1], Jing-Tang Chang [2] and Yu-Tse Lin [2]

[1] Department of Mechanical and Computer Aided Engineering, National Formosa University, Huwei, Yunlin County 63201, Taiwan; 40571201@gm.nfu.edu.tw or 10920110@gm.nfu.edu.tw
[2] Coating Department, Supati Corporation, Citong, Yunlin County 64747, Taiwan; jingtangc@gmail.com (J.-T.C.); 10420302@gm.nfu.edu.tw or d0875102@gm.nfu.edu.tw (Y.-T.L.)
* Correspondence: cckuo@nfu.edu.tw; Tel.: +886-5631-3492

Abstract: The Zr film microstructure is highly influenced by the energy of the plasma species during the deposition process. The influences of the discharge pulse width, which is the key factor affecting ionization of sputtered species in the high-power impulse magnetron sputtering (HiPIMS) process, on the obtained microstructure of films is investigated in this research. The films deposited at different argon pressure and substrate biasing are compared. With keeping the same average HiPIMS power and duty cycle, the film growth rate of the Zr film decreases with increasing argon pressure and enhancing substrate biasing. In addition, the film growth rate decreases with the elongating HiPIMS pulse width. For the deposition at 1.2 Pa argon, extending the pulse width not only intensifies the ion flux toward the substrate but also increases the fraction of highly charged ions, which alter the microstructure of films from individual hexagonal prism columns into a tightly connected irregular column. Increasing film density leads to higher hardness. Sufficient synchronized negative substrate biasing and longer pulse width, which supports higher mobility of adatoms, causes the preferred orientation of hexagonal α-phase Zr films from (0 0 0 2) to (1 0 $\bar{1}$ 1). Unlike the deposition at 1.2 Pa, highly charged ions are also found during the short HiPIMS pulse width at 0.8 Pa argon.

Keywords: zirconium; high-power impulse magnetron sputtering; pulse width

Citation: Kuo, C.-C.; Lin, C.-H.; Chang, J.-T.; Lin, Y.-T. Effect of Voltage Pulse Width and Synchronized Substrate Bias in High-Power Impulse Magnetron Sputtering of Zirconium Films. *Coatings* **2021**, *11*, 7. http://dx.doi.org/10.3390/coatings11010007

Received: 27 November 2020
Accepted: 21 December 2020
Published: 23 December 2020

1. Introduction

Zirconium (Zr) exhibits exceptional properties, such as low neutron absorption cross-section, high mechanical strength, high melting temperature, resistance to corrosion and oxidation [1–4]. Therefore, Zr can be used as an alloying agent or compound in materials. Its alloys, oxides and nitrides are widely used in many refractory and machining applications [1,3–5], including nuclear reactors [6–9], aerospace turbines [10], crucibles and furnaces [11]. Zirconium is also a non-toxic, biocompatible material for medical implants [12,13]. Its powder also can be used as explosive primers and catalysis [14]. Zirconium could be a potential source to fabricate high-k gate dielectrics in semiconductor field-effect transistors and a candidate for infrared reflectors [14,15]. Most of these Zr-contained alloy or compound films are deposited by applying physical vapor depositions (PVD) [4,5,15–21], parts are prepared by plasma spray and chemical vapor deposition [10,22]. The obtained film structure is significantly influenced by substrate material, interlayer, source material, negative substrate biasing and kinetic energy of generated species [16,19–21]. Since zirconium is a raw material for products in such a wide range of applications, and various deposition techniques of zirconium-contained coatings have been attempted and industrialized, knowing the properties and discharge behavior of zirconium sources is essential for the process control.

High-power impulse magnetron sputtering (HiPIMS) is a highly ionized physical vapor deposition technique, which is based on magnetron sputtering with delivering high-

power densities in pulses with a low duty cycle [23,24]. The high-power pulse mode enables a high-density plasma above the source cathode and enhances the ionization ratio of the sputtered source particles, which provides facilitation for altering the film microstructure through controlling the kinetic energy of incident ions and migration of adatoms via substrate biasing [25–27]. It allows the preparation of films with superior properties, especially compared to direct current magnetron sputtering [28,29]. This feature meets the demands of microstructural texturing for zirconium thin film preparation [16,19–21] and lowers down the deposition temperature for specific crystalline phases [30,31].

Although various HiPIMS power supplies or coating systems are commercialized for years [24], the discharge behavior for each different metal and the physics behind it are still in exploration [25–27,31–35]. Effects of pulse off time, substrate bias, and magnetic field on the HiPIMS deposition of zirconium-containing coatings have been reported [21,36,37], but the influences of discharge pulse width, deposition pressure, and applying synchronized substrate bias have not been revealed. In our previous work [38], it was found that the deposition pressure, the discharge pulse width significantly affects the energy of ions and the obtained chromium film structure. A synchronized pulsed substrate bias effectively prevents the bias voltage from dropping while the high-power pulse discharge initiates, as described in the literature [23,39]. This helps the improvement of the film density and the crystallinity through steady substrate bias voltage. Therefore, this work researched the influences of the HiPIMS discharge pulse width at two different argon deposition pressure on the microstructure of obtained zirconium films.

2. Materials and Methods

The deposition system and power supplies were described in our previous work of Cr films [38]. The source material was one rectangle zirconium target cathode (432 (L) × 76 (w) × 13 (h) mm^3) with an unbalanced magnetron and connected with the TRUMPF Hüttinger TruPlasma Bias 4010 G2 (TRUMPF, Ditzingen, Germany) in the unipolar negative voltage pulse mode. Two different substrate materials were used at the same time, SUS 304 stainless steel mirror plate with a size of 20 (w) × 30 (l) × 1 (h) mm^3 and Silicon wafer chips with a size of 1021 mm^2 (a) × 0.3 mm (h). The cleaning process, the position in the deposition chamber, and the argon glow discharge ion bombardment of substrate samples are the same as our previous work [38]. The deposition parameters for Zr films are shown in Table 1.

Table 1. Parameters for the deposition of zirconium films.

Deposition Parameters		Value
Atmosphere	Argon pressure (Pa)	0.8, 1.2
Target HiPIMS power	Average power (kW)	3
	Peak voltage (V)	−987~−877
	Peak current (A)	214~156
	Pulse frequency (Hz)	410, 105, 58
	Pulse width (μs)	60, 200, 400
	Pulse duty cycle (%)	~2.5
Zr ion bombardment	Synchronized bias voltage pulse	−1000 V (pulse width 120, 400, 800 μs)
	Bombardment time	40 s
Zr film deposition	Synchronized bias voltage pulse	Ground 0 V, −200 V (pulse width 120, 400, 800 μs)
	Deposition time	40 min
Deposition temperature (°C)		190~200

Note: high-power impulse magnetron sputtering (HiPIMS).

Rectangle high voltage pulses with three different pulse widths 60, 200 and 400 μs were, respectively, were applied to the source-target to initiate the sputtering of zirconium. The pulse voltage and the corresponding peak current on the target float between −987 to

−877 V due to the varying target conditions and the set deposition pressures. To simplify the conditions of varying voltage, current, and peak power of each pulse, the pulse frequencies were manually set with the same pulse duty cycle 2.5% to keep a constant target average power of 3 kW for all depositions.

Applying a pulsed substrate bias, which is synchronized with the target HiPIMS discharge pulse, is helpful to selectively attract ions and the charged species with a stable bias voltage and enables the target ion bombardment for a stronger film adhesion [23,38]. As the target HiPIMS pulse began, the substrate bias voltage pulse of–1000 V with a 2-fold pulse width of HiPIMS pulses was simultaneously applied in order to accelerate Zr ions to bombard the substrate. To minimize the roughness and temperature change on the substrate surface, the Zr ion bombardment is restricted to 40 s, and the substrate temperature was not over 200 °C. After ion bombardment, the substrate bias voltage then switched to 0 V (grounded) or pulsed −200 V directly without any gradient biasing to deposit a subsequent Zr film for 40 min. During the deposition, the optical emission spectra of HiPIMS discharge were recorded by applying an AvaSpec-ULS2048XL-EVO spectrometer (AVANTES, Apeldoorn, The Netherlands) with 1 s accumulation time.

A scanning electron microscope (SEM, S-4800 Cold Field Emission Scanning Electron Microscope, Hitachi, Tokyo, Japan) was used to observe the top and cross-sectional microstructures of deposited Zr films. Film thickness was estimated from cross-sectional images. The X-ray diffractometer (XRD, D8 Discover X-ray diffractometer, Bruker, Billerica, MA, USA) was utilized to characterize the crystallinity of the Zr films. The nanoindentations (A TTX-NH3 nanoindentation tester, Anton Paar, Graz, Austria) were carried out to evaluate the film hardness. Settings of analysis instruments were as the same as described in the references [38].

3. Results and Discussion

3.1. The Comparison between HiPIMS Discharge Behaviors of Zr at the Difference Deposition Pressure and Voltage Pulse Width

The current pulse shape of the Zr cathode with different HiPIMS voltage pulse width and under three different deposition pressures are shown in Figure 1. The current initially increases to the maximum in 20 to 50 µs. The higher the pressure is, the faster the current increases. This is due to the enhancement of ionization through increased species collisions at higher pressure [23–25]. For the pulse longer than 60 µs, the current decreases moderately after the maximum. Moreover, the current increases to about 150 µs. This second current peak could be attributed to the appearance of metal ions after the transformation from the argon sputtering stage into the self-sputtering stage [23–25]. The curves in Figure 1b,c are similar, but a drastically current drop occurred at about 150 µs on curves in Figure 1a. This current drop could be due to the gas rarefaction, and the pressure is too low to sustain the self-sputtering process [24]. The areas of current pulses of 1.2 Pa are slightly higher than those of 0.8 Pa but much higher than those of 0.13 Pa.

To confirm such difference among the excited ions at three deposition pressures and different pulse widths, the responded substrate current pulses are recorded by the built-in oscilloscope of the bias power supply while applying the synchronized −800 V substrate bias pulses with 1 ms pulse width. The substrate current represents the state of the incident ions toward the substrate. In order to clearly demonstrate the disparity, only three substrate current pulses of different HiPIMS pulse widths at each pressure are shown in Figure 2. The pulse width of 60 µs is shorter than the moment of the maximum current peak in Figure 1. The pulse width of 200 µs is just after the second current peak in Figure 1b,c, and the current drop in Figure 1a. The longest pulse width in this study is 400 µs. As shown in Figure 2, the area of the responded substrate current pulse extends with the target pulse width. Although the contributions of Ar or Zr ions on the substrate current remain indistinguishable, the extended area of current pulses indirectly evidences that the amount and the charge state of ions intensify with the pulse width. All the responded substrate current pulses in Figure 2 are broader than the corresponding target current pulse width in Figure 1. The peak currents of 200 µs and 400 µs in Figure 2 occur afterward

comparing to the relevant pulses in Figure 1. Moreover, the delay elongates with increasing deposition pressure from 0.13 Pa to 0.8 Pa. The delay between pulses at 0.8 and 1.2 Pa is indistinguishable. Such delay at different deposition pressure could be attributed to several reasons, including the duration of the ion recycling, the transition from gas sputtering into self-sputtering, and the flight of ions from target to the substrate [23,24,32,38,40–42]. At the beginning of each HiPIMS pulse, the strong negative voltage on the target attracts back a large fraction of the gas ions and sputtered metal ions (ion recycling), which restricts the fraction of ions that reach the substrate until the conditions of the discharge current runaway are fulfilled [23,24]. The responded substrate current of target pulse width 60 µs is much lower than those of target pulse width 200 and 400 µs at all three pressures. This implies the ion flux or the ionization ratio of the sputtered species could be much lower when the pulse width is short. The relatively much lower currents at 0.13 Pa shown in Figures 1a and 2a imply a lower ionization ratio of the Zr species, which is not a proper condition of the HiPIMS deposition of the Zr film. There is a current drop at about 200 µs in Figure 2a, which is consistent with Figure 1a. Therefore, pressures of 0.8 Pa and 1.2 Pa were chosen to deposit zirconium films for further experiments.

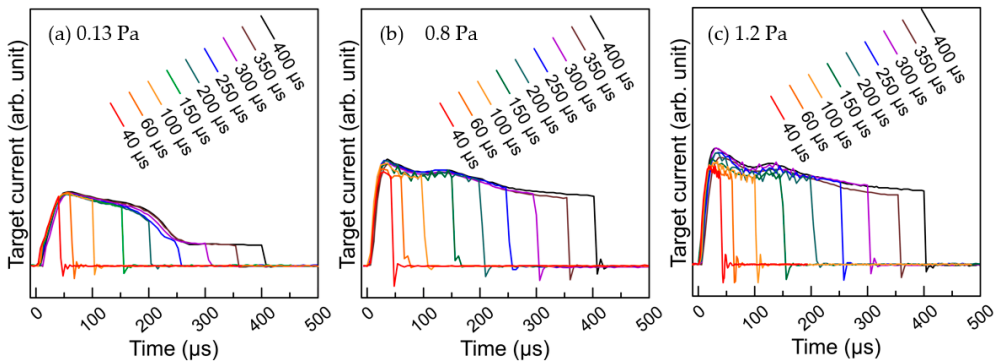

Figure 1. The single current pulse waveforms of the rectangular pulse voltages with different pulse widths for high-power impulse magnetron sputtering (HiPIMS) discharges on a Zr target in argon at (**a**) 0.13 Pa (**b**) 0.8 Pa and (**c**) 1.2 Pa.

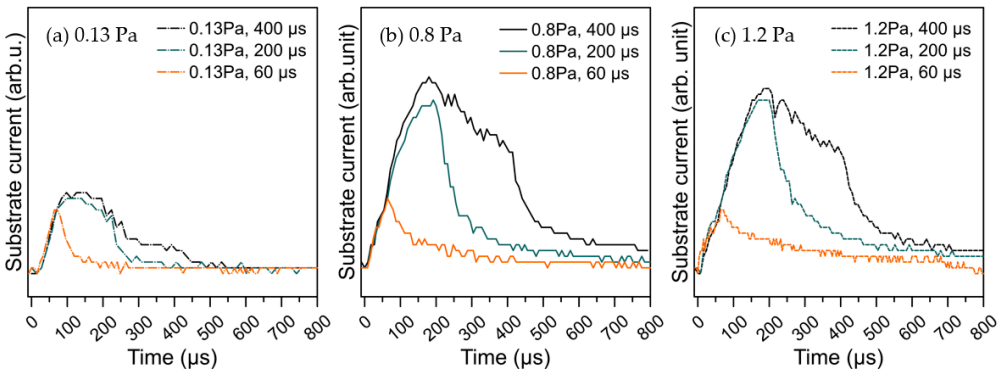

Figure 2. The responded substrate bias current pulse waveforms of a constant substrate bias pulse voltage of −800 V for 1 ms width, which are synchronized with the HiPIMS discharges pulse widths of the Zr target in argon at (**a**) 0.13 Pa (**b**) 0.8 Pa and (**c**) 1.2 Pa.

3.2. *Effects of the Pulse Width on the Zr Film Structure*

Figure 3 shows the top and cross-sectional SEM SE images of HiPIMS Zr films deposited with different pulse widths, 60, 200 and 400 µs at deposition pressure 1.2 Pa onto grounded silicon wafer chips (substrate bias 0 V). Three samples of the different pulse widths present different columnar cross-sectional features. The microstructures of the Zr films of 60 and 200 µs shown in Figure 3a,b are similar to the pulsed-DC deposited Zr films

at a temperature of 773 K [19]. These loosen columnar features are in the range of Zone 1 according to the structure zone model proposed by Anders based on Thornton's structure zone model [43]. The inter-columnar void between hexagon columns, which results from the shadowing effect, reduces. The hexagonal pointed top becomes more rounded, flatter and irregular, with an elongation of the pulse width. The microstructure of the Zr film of 400 μs in Figure 3c is in the range of Zone T. Similar trends were found in other reported HiPIMS Cr films [34,38].

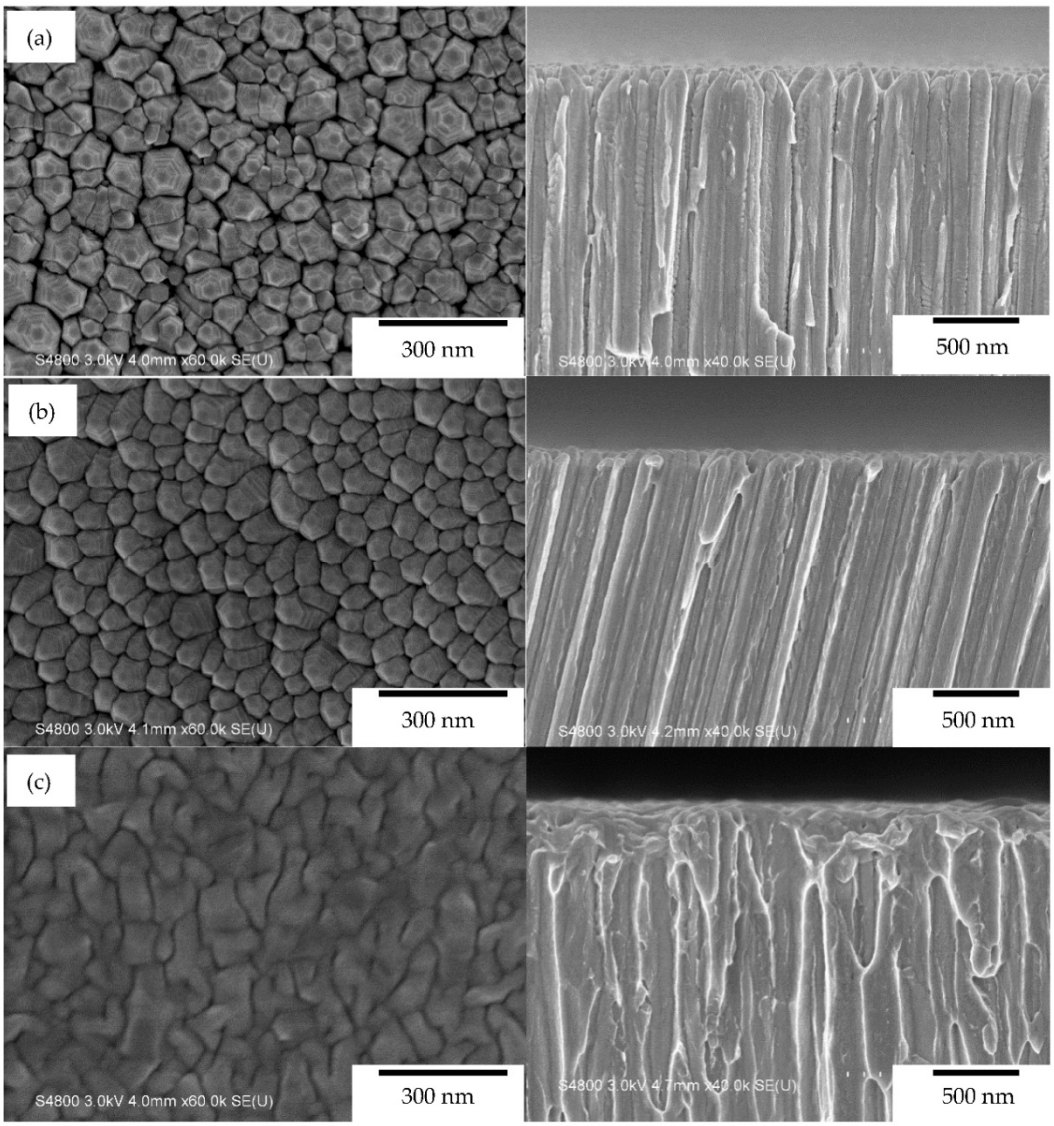

Figure 3. Top (left side) and cross-sectional (right side) SEM SE micrographs of Zr films deposited with the target pulse width of (**a**) 60 μs, (**b**) 200 μs, and (**c**) 400 μs, at the argon pressure of 1.2 Pa on the grounded (substrate bias 0 V) silicon wafer chips.

The density of excited ions and the portion of high energy ions both increase with the pulse peak power in a HiPIMS process [33]. Since the output voltage pulse waveform of the HiPIMS power in this work is near to a rectangular pulse with a voltage variation of 11%, the peak power can be considered in proportion to the current pulse width. The increased ion flux and ion energy provide higher mobility of adatom to diffuse further and to form a denser and crystalline structure [27,31]. The X-ray diffractograms of the deposited films in Figure 4 prove this assumption about the energy change of adatoms. There are only diffraction peaks of hexagonal close-packed α-phase of three films with different pulse

widths. Without applying substrate bias, the deposited Zr films tend to exhibit a preferred orientation of (0 0 0 2). Since the three films are all thicker than 4 μm, the influences of film thickness on crystal structure can be ignored [20]. The peak intensity of preferred orientation enhances with elongating the pulse width indicates that the crystallinity of films also increases with the pulse width.

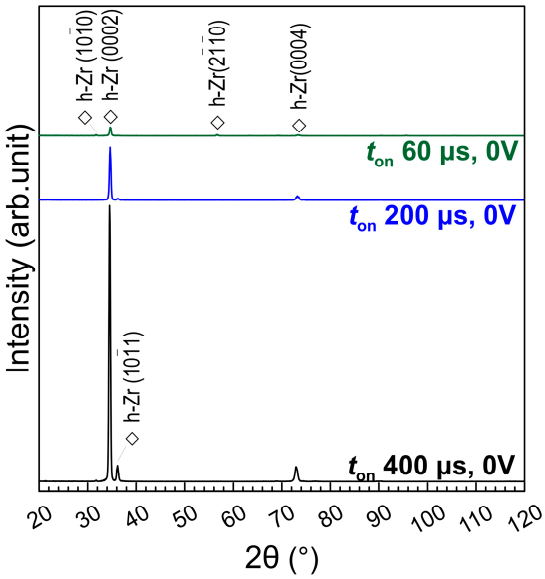

Figure 4. X-ray diffractograms of Zr films deposited at the argon pressure of 1.2 Pa and the substrate bias of 0 V with different HiPIMS pulse widths (t_{on}).

The estimated deposition rate of at pulse widths of 60, 200, and 400 μs are, respectively, 140, 151, and 157 nm/min. Even the average target power is kept at the same 3 kW, and the duty cycle is kept at the same 2.5%, the deposition rate increases with the pulse width. One possible reason is mentioned in the previous section. It usually requires several microseconds delay for the ion recycling process before the discharge current runaway is fulfilled [23,24] in each pulse. In the condition of the same duty cycle, the proportion of delay for a shorter pulse with a higher frequency is relatively increased, which results in a lower proportion for really releasing sputtered species toward the substrate.

3.3. Effects of Synchronized Pulse Substrate Bias on the Zr Film Structure

Figure 5 shows the top and cross-sectional SEM SE micrographs of the Zr films deposited with target different pulse widths, but the same synchronized pulse substrate bias of −200 V at 1.2 Pa. The microstructures of the three films with different pulse widths are similar and in the range of Zone 2 [43]. The boundaries of columns are closely connected with granular edges. Comparing with the microstructure of films shown in Figure 3, the films deposited with applying substrate bias of −200 V shown in Figure 5 exhibit relatively denser structures without inter-columnar voids. It demonstrates the incident charged species toward the substrate and deposited adatoms are entirely energized by negative substrate bias. On one hand, the similar microstructure in Figure 5 indicates that the ion energy enhancement by the negative substrate bias surpasses the effect of pulse width and peak power. On the other hand, applying adequate substrate bias can counteract the weakness of the lower ion energy for short pulse widths.

In Figure 6, the XRD patterns of three films deposited with a substrate bias of −200 V show strong diffraction peaks of crystalline α-phase. This again suggests that using the substrate bias will enhance the ion energy and improve the crystallinity. While using a longer pulse width or a negative substrate bias, the adatoms would be energized to migrate long distances to arrange a more ordered crystalline structure. The film of 60 μs exhibits the same preferred orientation of (0 0 0 2), but a much stronger diffraction peak. However, the

strongest peak of films of pulse width 200 and 400 μs with −200 V substrate bias changes to (1 0 $\bar{1}$ 1). Similar changes in the preferred orientation results by the substrate bias were found on metallic and nitride films [27,31,38,44–46]. Adatoms with higher mobility could migrate further on the planes which require longer diffusion distance [27,31], which promotes the epitaxial grain growth [32,33] and also lead to a finer grain structure [43,44]. The high ion-to-atom ratio and high ion bombardment also cause the recrystallization and consequent epitaxial growth of grains [45].

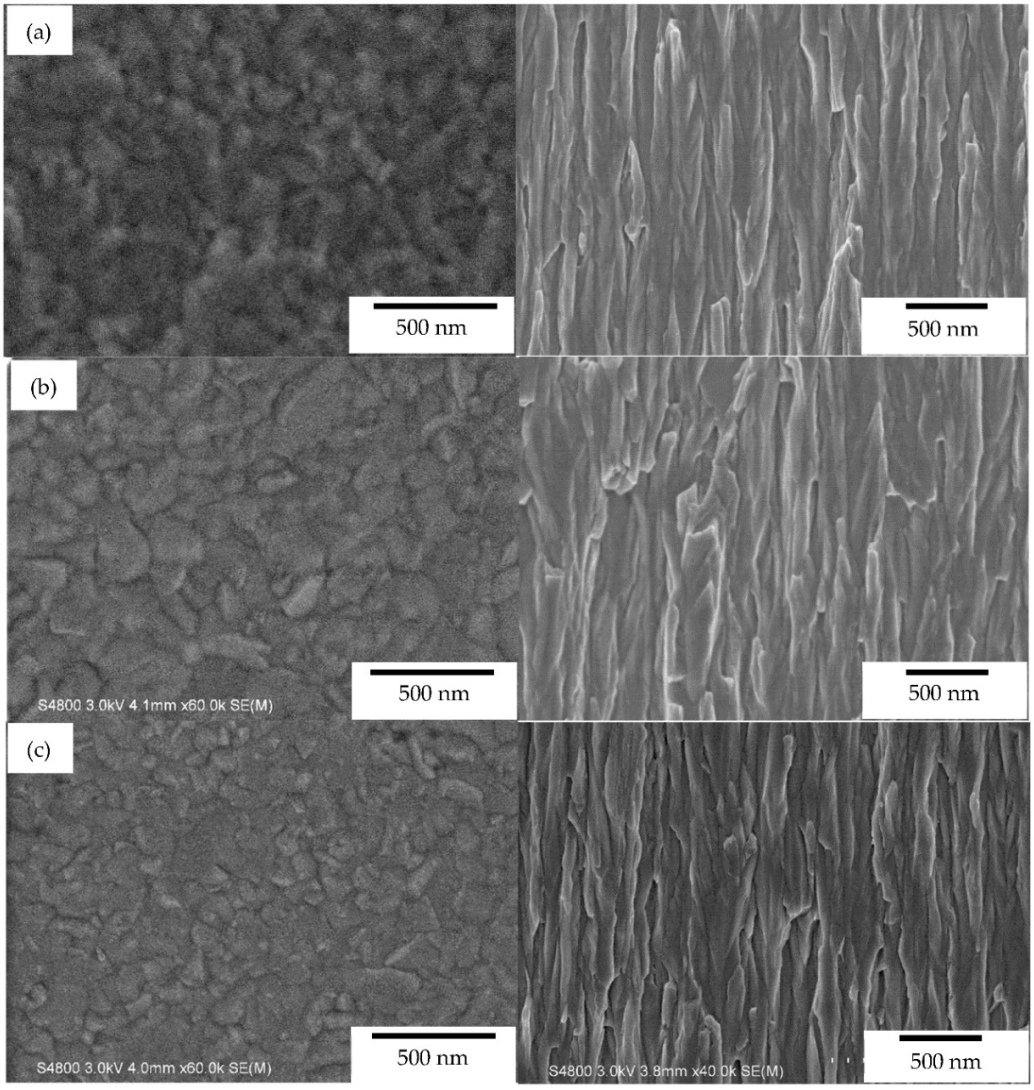

Figure 5. Top (left side) and cross-sectional (right side) SEM SE micrographs of Zr films deposited with the target pulse width of (**a**) 60 μs, (**b**) 200 μs, and (**c**) 400 μs, at the argon pressure of 1.2 Pa on the silicon wafer chips with applying synchronized substrate pulse bias −200 V.

The estimated deposition rate of pulse width 60, 200, and 400 μs with applying −200 V substrate bias are respectively 109, 126, and 138 nm/min. The deposition rate still increases with the pulse width when the −200 V substrate bias is applied. The deposition rates for films of −200 V substrate bias are about 28%, 19% and 13% lower than that of 0 V. This could be attributed to reducing void and the sputtering loss of adatoms. This difference between film growth rates of HiPIMS depositions with and without substrate bias voltage reduces with the target pulse width. This could be due to the increase of the film density with elongating the pulse width for films of substrate bias 0 V. The film hardness could be

an indirect proof of the increasing film density by extending the target pulse width and applying the negative substrate bias.

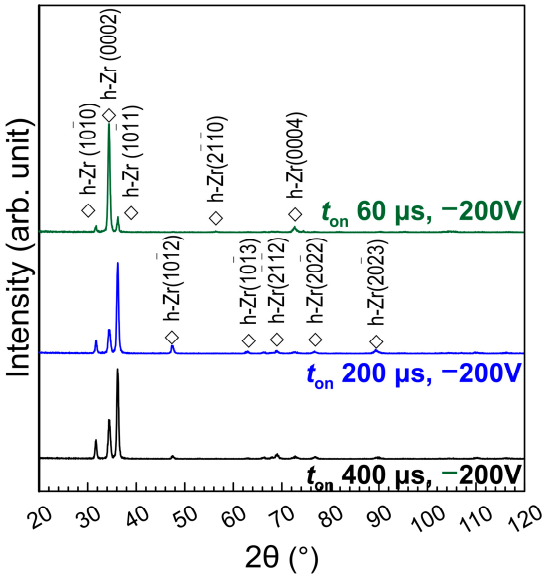

Figure 6. X-ray diffractograms of Zr films deposited at an argon pressure of 1.2 Pa and pulsed subscheme 200. V with different HiPIMS pulse widths (t_{on}).

Figure 7 shows the nanoindentation results of the Zr films deposited at a pressure of 1.2 Pa by applying different target pulse widths and negative substrate bias voltages. The film hardness of pulse width 200 and 400 μs are about 30% higher than that of pulse width 60 μs. This trend is consistent with the reported HiPIMS deposition of Cr films [35,38]; the film hardness increases with the peak power. Applying a negative substrate bias voltage enhances the film hardness significantly, from 15% to 32%. The increased film hardness for longer pulse width and applying substrate bias could be attributed to the elimination of inter-columnar voids shown in Figure 1. However, based on the Hall–Petch relation, the grown grain size, which countervails the benefit from increased film density, which may be the reason for the competitive hardness values for films of target pulse width 200 and 400 μs.

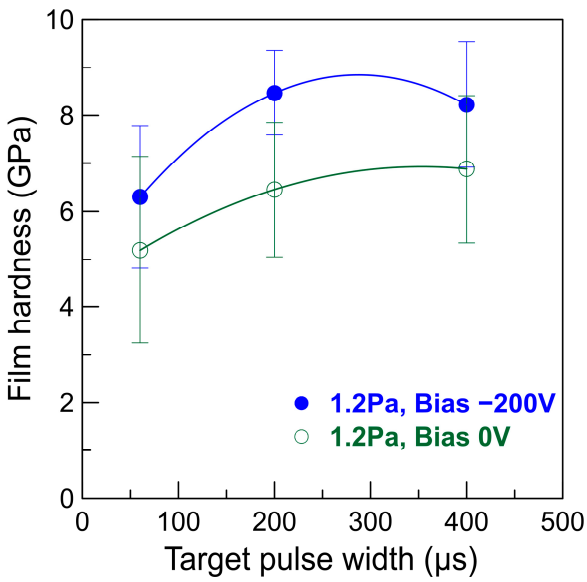

Figure 7. Film hardness versus the HiPIMS pulse width for Zr films deposited at the argon pressure of 1.2 Pa with and without negative substrate bias voltages.

3.4. Effects of Deposition Pressure on the Zr Film Structure

In previous work of Cr films, higher deposition pressure usually results in a lower deposition rate due to the increased scattering loss of sputtered species during the flight at high working pressure. The increase of scattering of sputtered particles with working pressure has been detailly investigated by Wu et al. [47]. In addition, the decrease of deposition rate reduces with elongating the pulse width [38]. In order to compare, Zr films of the different pulse widths were also prepared at a substrate bias of −200 V in a 0.8 Pa argon atmosphere. Figure 8 shows the top and cross-sectional morphologies of the Zr films of the working pressure of 0.8 Pa are shown. The microstructures of the three films are all in the range of Zone 2 and similar to those in Figure 5. The estimated deposition rate of pulse width 60, 200, and 400 μs are 118, 130, and 139 nm/min, which are slightly higher but very close to those of 1.2 Pa listed in the previous section. Furthermore, the film hardness of the three pulse widths is approximate about 7 GPa and slightly increases with the pulse width. This is different from the deposition of Cr films [38].

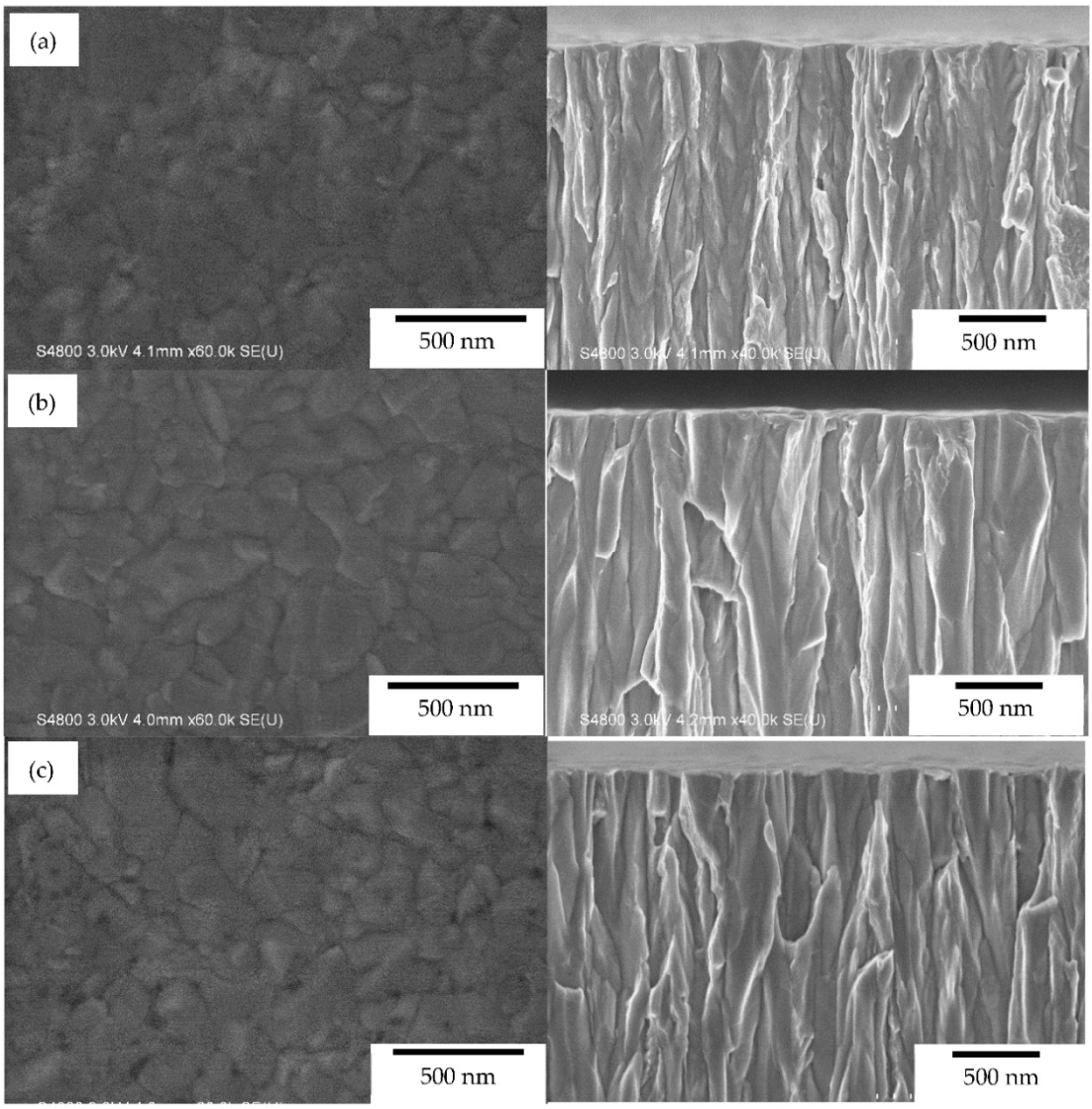

Figure 8. Top (left side) and cross-sectional (right side) SEM SE micrographs of Zr films deposited with the target pulse width of (**a**) 60 μs, (**b**) 200 μs, and (**c**) 400 μs, at the argon pressure of 0.8 Pa on the silicon wafer chips with applying synchronized substrate pulse bias −200 V.

The XRD patterns of the Zr films of 0.8 Pa, as shown in Figure 9, are similar to those in Figure 6. However, the relative intensity of peak (1 0 $\bar{1}$ 1) for all three pulse widths is stronger than those of 1.2 Pa. This implies that the ionization ratio and the energy of excited ions for 60 µs pulse width at 0.8 Pa could be higher than that at 1.2 Pa. To investigate the difference of excited plasma species in these two argon pressures. The optical emission spectra were recorded during the film deposition at different pulse widths and working pressures, as shown in Figure 10. At a pressure of 1.2 Pa (Figure 10b), the intensity of emission peaks with a wavelength shorter than 440 nm all intensify with elongating pulse width. This means that the ionization ratio and high charged ions increase with the pulse width.

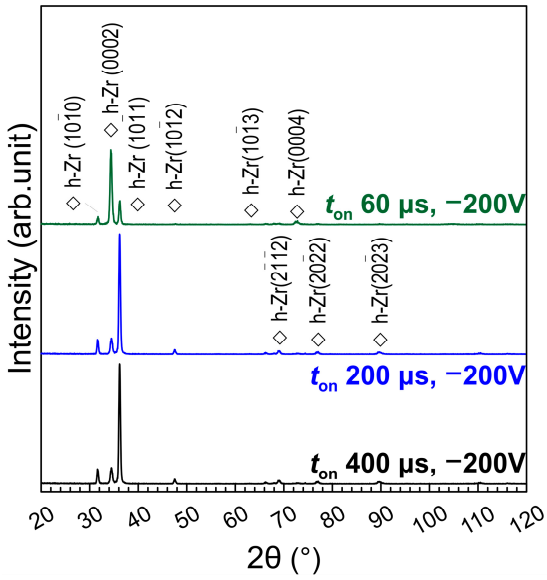

Figure 9. X-ray diffractograms of Zr films deposited at the argon pressure of 0.8 Pa and pulsed substrate bias of −200 V with different HiPIMS pulse widths (t_{on}).

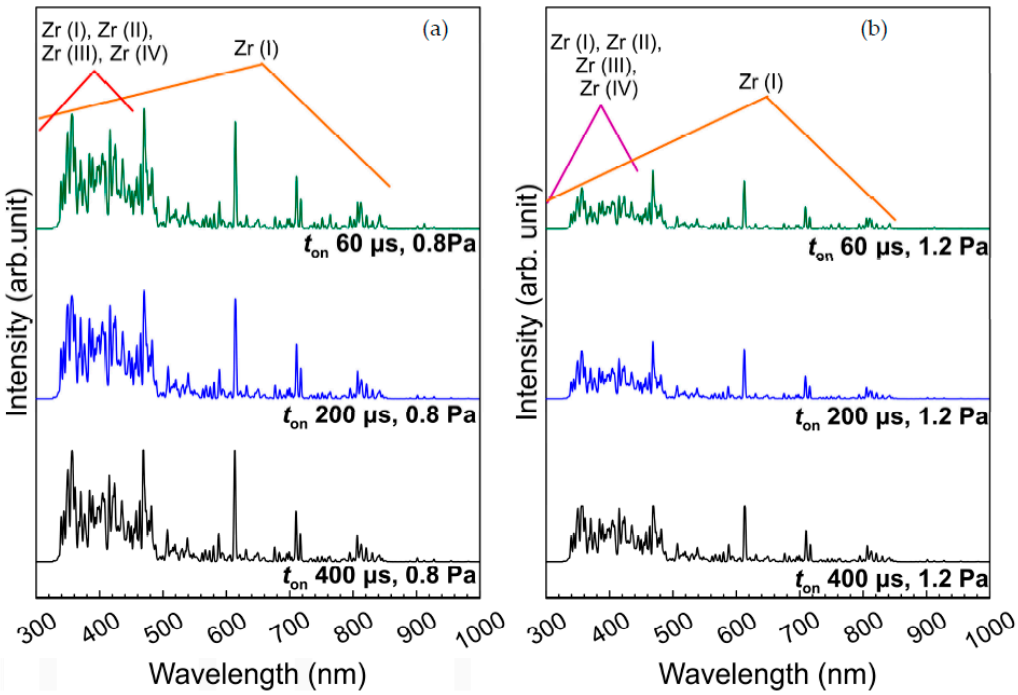

Figure 10. Optical emission spectra of the HiPIMS discharge of different pulse widths at the argon pressure of (**a**) 0.8 Pa and (**b**) 1.2 Pa.

Otherwise, the emission peaks with the wavelengths shorter than 440 nm are strong for all pulse widths at a pressure of 0.8 Pa. This reveals the ionization ratio of sputtered Zr species could be higher at a pressure of 0.8 Pa. This could be the reason for approximate hardness values for films of three pulse width. However, the substrate current curves in Figure 2b,c does not present a corresponding increase. The energy distribution of differently charged ions could be varied by the pulse width [42], pressure [48], and properties of source material [25]. The ion flux could also be varied by the pressure and the ejection angle [40]. It requires further investigation to reveal the mechanism.

By comparing with the HiPIMS deposition of titanium and chromium films [30,38], several phenomena of HiPIMS deposition, which are very different from those of direct current magnetron sputtering, were found. In the typical magnetron sputtering, the relationship between plasma power, pressure, working distance, and deposition rate of different elements are similar and can be easily estimated by referred to the reported sputtering yield vs. Ar^+ [49]. This relationship in HiPIMS deposition of different can be different, even contrary. For example, the sputtering yield vs. Ar^+ of chromium is twice that of those of zirconium and titanium. However, the deposition rate of zirconium is four times as chromium and twice of titanium with the same HiPIMS deposition parameters. This could be a result of compromised and synergistic influences of pressure, ejection angle, self-sputtering yield, ionization ratio [23]. This work preliminarily indicates the influences of discharge pulse width, deposition pressure and substrate bias on the HiPIMS deposition of zirconium film. The results can be used to evaluate the settings of deposition pressure and pulse width for HiPIMS depositing zirconium alloys or compounds by utilizing multi-target co-sputtering or composite targets for desired compositions and texture. For instance, a long pulse width could be the better choice to deposit crystalline metallic films on a low thermal tolerant and electrically insulated polymer substrate. Short pulse width could minimize the target poisoning effect in a reactive HiPIMS deposition of zirconium compounds, and the lower deposition pressure could be the better choice for a higher ion flux and less hysteresis [24].

4. Conclusions

This research preliminarily investigates the influences of basic parameter settings, including discharge pulse width, deposition pressure and substrate bias, on the high-power impulse magnetron sputtering deposition of zirconium film with the same average power and pulse duty cycle.

Without applying the substrate bias, the inter-column gaps and voids reduce with elongating of the discharge pulse width and individual hexagon columns. The crystallinity and preferred orientation of films also enhance the discharge pulse width due to the enhanced ionization ratio of sputtered species. Applying the synchronized negative substrate bias voltage effectively intensifies the energy of sputtered species and adatoms, in order to alter the loosened columnar film microstructure into a more crystalline, epitaxial granular, and denser one. In the case of the densified film microstructure, the film hardness increases with the pulse width and negative substrate bias. The deposition rates of the Zr thin films at working 0.8 Pa are higher but close to those of 1.2 Pa. The Zr films deposited with different pulse widths at 0.8 Pa exhibit similar microstructure, and preferred orientations are similar to those of 1.2 Pa, but the fraction of $(1\ 0\ \bar{1}\ 1)$ orientation is increased. This could be attributed to the higher ionization ratio at 0.8 Pa. These trends can help to estimate proper settings of deposition pressure, discharge pulses, and substrate bias to synthesize zirconium-contained alloys and compounds, with the desired texture and composition, by using multi-target co-sputtering or composite target.

Author Contributions: Conceptualization, C.-C.K. and J.-T.C.; data curation, C.-H.L.; investigation, J.-T.C., C.-H.L., and Y.-T.L.; methodology, C.-C.K. and J.-T.C.; project administration, C.-C.K.; supervision, C.-C.K.; visualization, J.-T.C.; writing—original draft, J.-T.C. and C.-C.K.; writing—review and editing, C.-C.K. All authors have read and agreed to the published version of the manuscript.

Funding: This research received no external funding.

Institutional Review Board Statement: Not applicable.

Informed Consent Statement: Not applicable.

Data Availability Statement: Data is contained within the article.

Acknowledgments: The authors wish to thank Supati Cooperation for financial support. Precision Instrument Support Center of Feng Chia University is also acknowledged for the microstructure analysis instruments.

Conflicts of Interest: The authors declare no conflict of interest.

References

1. Pierson, H.O. *Handbook of Refractory Carbides and Nitrides*, 1st ed.; Noyes Publications: Westwood, NJ, USA, 1996; pp. 55–80.
2. Fisher, E.S.; Renken, C.J. Single-crystal elastic moduli and the hcp→bcc transformation in Ti, Zr, and Hf. *Phys. Rev.* **1964**, *135*, A482. [CrossRef]
3. Toth, L.E. *Transition Metal. Carbides and Nitrides*; Academic Press: New York, NY, USA, 1971; pp. 1–25.
4. Tung, H.-M.; Wu, P.-H.; Yu, G.-P.; Huang, J.-H. Microstructures, mechanical properties and oxidation behavior of vacuum annealed TiZrN thin films. *Vacuum* **2015**, *115*, 12–18. [CrossRef]
5. Lugscheider, E.; Knotek, O.; Barimani, C.; Leyendecker, T.; Lemmer, O.; Wenke, R. PVD hard coated reamers in lubricant-free cutting. *Surf. Coat. Technol.* **1999**, *112*, 146–151. [CrossRef]
6. Ashcheulov, P.; Skoda, R.; Skarohlid, J.; Taylor, A.; Fendrych, F.; Kratochvílová, I. Layer protecting the surface of zirconium used in nuclear reactors. *Recent. Pat. Nanotech.* **2016**, *10*, 59–65. [CrossRef] [PubMed]
7. Hollis, K.J.; Hawley, M.E.; Dickerson, P.O. Characterization of thermal diffusion related properties in plasma sprayed zirconium coatings. *J. Therm. Spray Techn.* **2012**, *21*, 409–415. [CrossRef]
8. Hollis, K.J. Zirconium diffusion barrier coatings for uranium fuel used in nuclear reactors. *Adv. Mater. Process.* **2010**, *168*, 57–59.
9. Kang, Y.C.; Milovancev, M.M.; Clauss, D.A.; Lange, M.A.; Ramsier, R.D. Ultra-high vacuum investigation of the surface chemistry of zirconium. *J. Nucl. Mater.* **2000**, *281*, 57–64. [CrossRef]
10. Darolia, R. Thermal barrier coatings technology: Critical review, progress update, remaining challenges and prospects. *Int. Mater. Rev.* **2013**, *58*, 315–348. [CrossRef]
11. Northwood, D.O. The development and applications of zirconium alloys. *Mater. Des.* **1985**, *6*, 58–70. [CrossRef]
12. Thomsen, P.; Larsson, C.; Ericson, L.E.; Sennerby, L.; Lausmaa, J.; Kasemo, B. Structure of the interface between rabbit cortical bone and implants of gold, zirconium and titanium. *J. Mater. Sci. Mater. Med.* **1997**, *8*, 653–665. [CrossRef]
13. Mehjabeen, A.; Song, T.; Xu, W.; Tang, H.P.; Qian, M. Zirconium Alloys for Orthopaedic and Dental Applications. *Adv. Eng. Mater.* **2018**, *20*, 1800207. [CrossRef]
14. Wu, H.-C.; Huang, C.-J.; Youh, M.-J.; Tseng, C.-L.; Chen, H.-T.; Li, Y.-Y.; Sakoda, A. Thin-walled carbon nanotubes grown using a zirconium catalyst. *Carbon* **2010**, *48*, 1897–1901. [CrossRef]
15. Usmani, B.; Vijay, V.; Chhibber, R.; Dixit, A. Optimization of sputtered zirconium thin films as an infrared reflector for use in spectrally-selective solar absorbers. *Thin Solid Film.* **2017**, *627*, 17–25. [CrossRef]
16. Lim, J.-W.; Bae, J.W.; Zhu, Y.F.; Lee, S.; Mimura, K.; Isshiki, M. Improvement of Zr film purity by using a purified sputtering target and negative substrate bias voltage. *Surf. Coat. Technol.* **2006**, *201*, 1899–1901. [CrossRef]
17. Baudry, A.; Boyer, P.; Brunel, M.; Luche, M.C. Structure and magnetic behaviour of holmium-zirconium multilayers. *J. Phys. Condens. Matter.* **2000**, *12*, 3719. [CrossRef]
18. Smardz, L. Structure and magnetic properties of Fe/Zr multilayers. *J. Alloy. Compd.* **2005**, *395*, 17. [CrossRef]
19. Singh, A.; Kuppusami, P.; Thirumurugesan, R.; Ramaseshan, R.; Kamruddin, M.; Dash, S.; Ganesan, V.; Mohandas, E. Study of microstructure and nanomechanical properties of Zr films prepared by pulsed magnetron sputtering. *Appl. Surf. Sci.* **2011**, *257*, 9909–9914. [CrossRef]
20. Chakraborty, J.; Kumar, K.K.; Mukherjee, S.; Ray, S.K. Stress, texture and microstructure of zirconium thin films probed by X-ray diffraction. *Thin Solid Film.* **2008**, *516*, 8479–8486. [CrossRef]
21. Luo, H.; Gao, F.; Billard, A. Tunable microstructures and morphology of zirconium films via an assist of magnetic field in HiPIMS for improved mechanical properties. *Surf. Coat. Technol.* **2019**, *374*, 822–832. [CrossRef]
22. Ul-Hamid, A. The effect of deposition conditions on the properties of Zr-carbide, Zr-nitride and Zr-carbonitride coatings—A review. *Mater. Adv.* **2020**, *1*, 988–1011. [CrossRef]
23. Lundin, D.; Minea, T.; Gudmundsson, J.T. (Eds.) *High Power Impulse Magnetron Sputtering: Fundamentals, Technologies, Challenges and Applications*; Elsevier: Amsterdam, The Netherlands, 2019; ISBN 9780128124543.
24. Anders, A. Tutorial: Reactive high power impulse magnetron sputtering (R-HiPIMS). *J. Appl. Phys.* **2017**, *121*, 171101. [CrossRef]
25. Anders, A.; Andersson, J.; Ehiasarian, A. High power impulse magnetron sputtering: Current-voltage-time characteristics indicate the onset of sustained self-sputtering. *J. Appl. Phys.* **2007**, *102*, 113303. [CrossRef]
26. Kouznetsov, V.; Macak, K.; Schneider, J.; Helmersson, U.; Petrov, I. Hybrid HIPIMS and DC magnetron sputtering deposition of TiN coatings: Deposition rate, structure and tribological properties. *Surf. Coat. Technol.* **1999**, *12*, 290. [CrossRef]

27. Machunze, R.; Ehiasarian, A.; Tichelaar, F.; Janssen, G.; Ehiasarian, A. Stress and texture in HIPIMS TiN thin films. *Thin Solid Film.* **2009**, *518*, 1561–1565. [CrossRef]
28. Samuelsson, M.; Lundin, D.; Jensen, J.; Raadu, M.A.; Gudmundsson, J.T.; Helmersson, U. On the film density using high power impulse magnetron sputtering. *Surf. Coat. Technol.* **2010**, *205*, 591–596. [CrossRef]
29. Kuo, C.C.; Lin, Y.T.; Chan, A.; Chang, J.T. High Temperature Wear Behavior of Titanium Nitride Coating Deposited Using High Power Impulse Magnetron Sputtering. *Coatings* **2019**, *9*, 555. [CrossRef]
30. West, G.; Kelly, P.; Barker, P.; Mishra, A.; Bradley, J. Measurements of Deposition Rate and Substrate Heating in a HiPIMS Discharge. *Plasma Process. Polym.* **2009**, *6*, S543–S547. [CrossRef]
31. Elmkhah, H.; Attarzadeh, F.; Fattah-alhosseini, A.; Kim, K.H. Microstructural and electrochemical comparison between TiN coatings deposited through HIPIMS and DCMS techniques. *J. Alloy. Compd.* **2018**, *735*, 422–429. [CrossRef]
32. Greczynski, G.; Lu, J.; Jensen, J.; Bolz, S.; Kölker, W.; Schiffers, C.; Lemmer, O.; Greene, J.E.; Hultman, L. A review of metal-ion-flux-controlled growth of metastable TiAlN by HIPIMS/DCMS co-sputtering. *Surf. Coat. Technol.* **2014**, *257*, 15–25. [CrossRef]
33. Vetushka, A.; Ehiasarian, A.P. Plasma dynamic in chromium and titanium HIPIMS discharges. *J. Phys. D Appl. Phys.* **2008**, *41*, 015204. [CrossRef]
34. Ferreira, F.; Serra, R.; Oliveira, J.C.; Cavaleiro, A. Effect of peak target power on the properties of Cr thin films sputtered by HiPIMS in deep oscillation magnetron sputtering (DOMS) mode. *Surf. Coat. Technol.* **2014**, *258*, 249–256. [CrossRef]
35. Gudmundsson, J.T.; Alami, J.; Helmersson, U. Spatial and temporal behavior of the plasma parameters in a pulsed magnetron discharge. *Surf. Coat. Technol.* **2002**, *161*, 249–256. [CrossRef]
36. Sønderby, S.; Aijaz, A.; Helmersson, U.; Sarakinos, K.; Eklund, P. Deposition of yttria-stabilized zirconia thin films by high power impulse magnetron sputtering and pulsed magnetron sputtering. *Surf. Coat. Technol.* **2014**, *240*, 1–6. [CrossRef]
37. Zhao, X.L.; Jin, J.; Cheng, J.C.; Lee, J.W.; Wu, K.H.; Liu, K.C. Effect of pulsed off-times on the reactive HiPIMS preparation of zirconia thin films. *Vacuum* **2015**, *118*, 38–42. [CrossRef]
38. Kuo, C.C.; Lin, C.H.; Lin, Y.T.; Chang, J.T. Effects of Cathode Voltage Pulse Width in High Power Impulse Magnetron Sputtering on the Deposited Chromium Thin Films. *Coatings* **2020**, *10*, 542. [CrossRef]
39. Zuo, X.X.; Ke, P.P.; Chen, R.; Li, X.; Odén, M.; Wang, A. Discharge state transition and cathode fall thickness evolution during chromium HiPIMS discharge. *Phys. Plasmas* **2017**, *24*, 083507. [CrossRef]
40. Horwat, D.; Anders, A. Compression and strong rarefaction in high power impulse magnetron sputtering discharges. *J. Appl. Phys.* **2010**, *108*, 123306. [CrossRef]
41. Tsukamoto, K.; Tamura, T.; Matsusaki, H.; Tona, M.; Yamamoto, H.; Nakagomi, Y.; Nishida, H.; Hirai, Y.; Nishimiya, N.; Sanekata, M.; et al. Time-of-flight mass spectrometric diagnostics for ionized and neutral species in high-power pulsed magnetron sputtering of titanium. *Jpn. J. Appl. Phys.* **2020**, *59*, SHHB05. [CrossRef]
42. Bohlmark, J.; Lattemann, M.; Gudmundsson, J.T.; Ehiasarian, A.P.; Gonzalvo, Y.A.; Brenning, N.; Helmersson, U. The ion energy distributions and ion flux composition from a high power impulse magnetron sputtering discharge. *Thin Solid Film.* **2006**, *515*, 1522–1526. [CrossRef]
43. Anders, A. A structure zone diagram including plasma-based deposition and ion etching. *Thin Solid Film.* **2010**, *518*, 4087–4090. [CrossRef]
44. Alami, J.; Maric, Z.; Busch, H.; Klein, F.; Grabowy, U.; Kopnarski, M. Enhanced ionization sputtering: A concept for superior industrial coatings. *Surf. Coat. Technol.* **2014**, *255*, 43–51. [CrossRef]
45. Mahieu, S.; Depla, D. Reactive sputter deposition of TiN layers: Modelling the growth by characterization of particle fluxes towards the substrate. *J. Phys. D Appl. Phys.* **2009**, *42*, 053002. [CrossRef]
46. De Monteynard, A.; Schuster, F.; Billard, A.; Sanchette, F. Properties of chromium thin films deposited in a hollow cathode magnetron powered by pulsed DC or HiPIMS. *Surf. Coat. Technol.* **2017**, *330*, 241–248. [CrossRef]
47. Wu, S.; Chen, H.; Du, X.; Liu, Z. Effect of deposition power and pressure on rate deposition and resistivity of titanium thin films grown by DC magnetron sputtering. *Spectrosc. Lett.* **2016**, *49*, 514–519. [CrossRef]
48. Hippler, R.; Cada, M.; Stranak, V.; Helm, C.A.; Hubicka, Z. Pressure dependence of singly and doubly charged ion formation in a HiPIMS discharge. *J. Appl. Phys.* **2019**, *125*, 013301. [CrossRef]
49. Seshan, K. (Ed.) *Handbook of Thin Film Deposition*, 3rd ed.; Elsevier: Amsterdam, The Netherlands, 2012; p. 53. ISBN 978-1-4377-7873-1.